Carbohydrate Polymers 113 (2014) 166–173

Contents lists available at ScienceDirect

Carbohydrate Polymers

journal homepage: www.elsevier.com/locate/carbpol

Grafting of β-cyclodextrin to magnetic graphene oxide via ethylenediamine and application for Cr(VI) removal

Hui Wang[a,b], Yun-guo Liu[a,b,*], Guang-ming Zeng[a,b], Xin-jiang Hu[a,b], Xi Hu[a,b], Ting-ting Li[a,b], Hua-ying Li[a,b], Ya-qin Wang[a,b], Lu-hua Jiang[a,b]

[a] College of Environmental Science and Engineering, Hunan University, Changsha 410082, PR China
[b] Key Laboratory of Environmental Biology and Pollution Control (Hunan University), Ministry of Education, Changsha 410082, PR China

ARTICLE INFO

Article history:
Received 24 October 2013
Received in revised form 30 March 2014
Accepted 1 July 2014
Available online 17 July 2014

Keywords:
Ethylenediamine
β-Cyclodextrin
Magnetic graphene oxide
Cr(VI)
Aniline
Removal

ABSTRACT

A novel β-cyclodextrin (β-CD) polymer adsorbent named β-cyclodextrin/ethylenediamine/magnetic graphene oxide (CD-E-MGO) was synthesized for decontamination of Cr(VI) from aqueous solution. The sorption kinetics, isotherms and thermodynamics, as well as the effects of pH, aniline and ionic strength on the sorption process were investigated. The results indicated that CD-E-MGO could effectively remove Cr(VI) from aqueous solution and the sorption data could be well described by pseudo-second-order and Langmuir models. The intraparticle diffusion study indicated that intraparticle diffusion was not the only rate-limiting step. Thermodynamic parameters revealed that the sorption reaction was an endothermic and spontaneous process. The decontamination of Cr(VI) was influenced by solution pH and ionic strength. In the system with aniline, the Cr(VI) sorption was improved at low pH values but reduced at high pH values. These results are important for estimating and optimizing the removal of metal ions by CD-E-MGO composite.

1. Introduction

Many organic and inorganic materials, such as activated carbon (Daifullah, Yakout, & Elreefy, 2007), graphene (Wu et al., 2011; Xu, Wang, & Zhu, 2012), purolite (Balan, Volf, & Bilba, 2013), β-cyclodextrin (Ozmen, Sezgin, Yilmaz, & Yilmaz, 2008), and chitosan (Hu et al., 2011), have been applied to remove heavy metal ions and organic substances. β-CD produced from the enzymatic degradation of starch by bacteria is a doughnut-shape cyclic oligosaccharide with a hydrophilic exterior and hydrophobic internal cavity (Ozmen et al., 2008; Pan et al., 2011). It is widely known that β-CD can form inclusion complexes with various organic compounds and metal ions in its hydrophobic cavity through host–guest interactions (Chen, Chen, & Chung, 2007; Szejtli, 1998). Besides, the hydroxyl groups on β-CD are known to form stable complexes with various metal ions. Therefore the β-CD may be favorable for contaminants removal from wastewaters. However, β-CD can be dispersed in aqueous media due to its hydrophilic exterior, so it is difficult to be separated from the solution using traditional separation methods after the sorption process, which may increase the cost of industrial application and/or cause the treated water to be re-polluted (Hu et al., 2013). Therefore, many researchers undertook a lot of attempts to graft β-CD on some supports for removal of organic compounds and heavy metal ions, such as grafting β-CD onto attapulgite (Pan et al., 2011), chitosan (Fan et al., 2012) and Fe_3O_4 (Badruddoza, Shawon, Daniel, Hidajat, & Uddin, 2013). These materials can be easily separated from the reaction medium and reused in next sorption cycle.

Graphene oxide (GO), also called graphite oxide sheet, is a two dimensional nanomaterial prepared from chemical oxidation of natural graphite (Allen, Tung, & Kaner, 2009; Chen et al., 2011; Hu et al., 2013). The oxidation process of graphite to GO can introduce abundant oxygen-containing functional groups such as epoxy, carbonyl, hydroxyl and carboxyl on the GO surfaces (Madadrang et al., 2012). These groups and large specific surface area make GO a superb platform for loading magnetic nanoparticles and grafting β-CD (Li et al., 2012). The integration of magnetic properties into GO can provide advantage of easy solid–liquid separation, but it has been found to have some negative effects on the sorption capacity of the GO (Li et al., 2012). The main reason for the loss of sorption capacity is that some sorption sites on the surfaces of GO are taken up by the magnetic nanoparticles. In order to increase the sorption ability, a great number of GO derivates have been obtained

* Corresponding author at: College of Environmental Science and Engineering, Hunan University, Changsha 410082, PR China. Tel.: +86 731 88649208; fax: +86 731 88822829.
E-mail address: hnuese@126.com (Y.-g. Liu).

http://dx.doi.org/10.1016/j.carbpol.2014.07.014
0144-8617/

by grafting new chemical substances such as sulfanilic acid (Hu et al., 2013), EDTA (Madadrang et al., 2012) and ethylenediamine (Ma et al., 2012) on GO backbone. Guo et al. (2010) and Guo, Guo, Li, Wang, and Dong (2011) have prepared the cyclodextrin-graphene hybrid nanosheets by reacting GO with cyclodextrin in the presence of hydrazine. On the basis of the above considerations, we suspect that grafting β-CD onto magnetic graphene oxide (MGO) will offer the possibility to combine the high sorption capacity of β-CD and the separation convenience of MGO. Ethylenediamine, the simplest 1,2-diamine, has similar physical–chemical properties to hydrazine. Besides, the amino groups of ethylenediamine are known to form stable complexes with various heavy metals. Therefore, in this work, we fabricated a novel β-CD polymer named CD-E-MGO by grafting β-CD onto MGO through the ethylenediamine, and applied it as a sorbent to remove Cr(VI) from aqueous solution.

Generally, some industrial wastewaters contain not only heavy metal ions but also high concentrations of organic substances and salts, which may affect the removal of heavy metal ions (Xu et al., 2012). Aniline is an important chemical substance for its wide applications in the manufacture of dyestuffs, rubbers, pesticides, plastics and paints (Lin, Zhang, Luo, Zhang, & Zhou, 2011). There is a high possibility that aniline and Cr(VI) ions exist in mixed contaminant systems. The aniline in wastewater may affect the sorption behaviors of Cr(VI) ions on CD-E-MGO due to that it can form stable complexes with Cr(VI) ions and interact with CD-E-MGO in aquatic systems. Furthermore, there are always some common ions in wastewater, such as Ca^{2+}, K^{+}, Na^{+}, Cl^{-}, and $NO_3{}^{-}$, which may also have influences on the heavy metals sorption processes (Xu et al., 2012). Therefore, it is significant to study the influences of aniline and ionic strength on the decontamination of Cr(VI) by CD-E-MGO.

The objectives of this study were to: (1) prepare and characterize CD-E-MGO composite and apply it as an sorbent to remove Cr(VI) from aqueous solution; (2) discuss the sorption mechanisms with kinetic, isotherm and thermodynamic models; (3) evaluate the effects of process parameters on Cr(VI) removal; (4) investigate the effects of aniline and ionic strength on Cr(VI) decontamination.

2. Materials and methods

2.1. Materials

β-CD was supplied by Tianjin Guangfu Chemical Preparation Co., Ltd. Ethylenediamine was purchased from Shanghai Chemical Reagents Factory. Graphite powder was obtained from Tianjin Hengxin Chemical Preparation Co., Ltd. Aniline was provided by Tianjin Fuchen Chemical Reagents Factory. All other reagents used in this study were analytical grade.

GO was prepared by using a modified Hummers method from the natural graphite powder (Hu et al., 2013; Yang et al., 2010). Briefly, graphite powder was first preoxidized by concentrated H_2SO_4, $K_2S_2O_8$ and P_2O_5. Then the obtained preoxidized graphite was oxidized by the concentrated H_2SO_4, $KMnO_4$ and $NaNO_3$. After that, 30% H_2O_2 was added to eliminate the excess $MnO_4{}^{-}$, and the products were rinsed with HCl (10%) and Milli-Q water and then sonicated for 2 h. The MGO was prepared by coprecipitation method (Wang et al., 2013). Fe^{3+} and Fe^{2+} (molar ratio 2:1) were mixed in the GO solution with addition of ammonia solution to form Fe_3O_4-GO composite (MGO). The CD-E-MGO was obtained by reacting β-CD with MGO through ethylenediamine at 80 °C for 24 h (Che, Shen, & Xiao, 2010; Guo et al., 2010, 2011; Ma et al., 2012; Ohashi, Hiraoka, & Yamaguchi, 2006). The resulted paste was washed repeatedly with Milli-Q water until pH was about 7.0 and finally stored at room temperature. Detailed processes are illustrated in the Supplementary data, and the preparation sketch of CD-E-MGO is shown in Fig. 1.

2.2. Characterization

The XRD pattern was recorded on an X-ray diffractometer (Rigaku D/max-2500, Japan) with Cu*K*a radiation. FT-IR spectrum of CD-E-MGO was measured on a spectrophotometer (Varian 3100, USA) using the KBr pellet technique. Raman spectra were carried out by using a Raman spectrometer (Labram-010, FAR). The magnetic property was characterized by magnetization curve using a vibrating sample magnetometer (Lake Shore 7410, USA). The XPS measurements were performed using an ESCALAB 250Xi X-ray photoelectron spectrometer (Thermo Fisher, USA). The zeta potentials of CD-E-MGO were measured at different pH by Zetasizer Nano ZS (ZEN3690, Malvern, UK).

2.3. Sorption experiments

All batch sorption experiments were performed in an incubator shaker with a shaking speed of 180 rpm. The stock solution (1000 mg/L) of Cr(VI) was prepared by dissolving 2.829 g $K_2Cr_2O_7$ in 1000 mL Milli-Q water in a volumetric flask. The solutions of different Cr(VI) concentrations used in batch experiments were obtained by diluting the stock solution. For all the sorption experiments, the suspension of MGO or CD-E-MGO was added to achieve the desired concentrations of the different components. The pH was adjusted to desired values by adding negligible volumes of NaOH or HCl. After being mixed for 24 h, the mixture was separated by a permanent magnet. Residual Cr(VI) and aniline concentrations in the supernatant were determined by an UV–vis spectrophotometer (Pgeneral T6, Beijing) at 540 nm according to the National Standard of the People's Republic of China (NSPRC, 1987) and 280 nm (Guo, Li, Liu, Yin, & Li, 2009), respectively. The sorption capacity (q_e) of CD-E-MGO for Cr(VI) was calculated from the difference between the initial concentration (C_0) and the equilibrium concentration (C_e) [$q_e = (C_0 - C_e) \times V/m$] (here, V is the volume of the suspension and m is the mass of CD-E-MGO).

3. Results and discussion

3.1. Characterization of CD-E-MGO

The XRD pattern of CD-E-MGO is shown in Fig. 2(a). The intense diffraction peaks at the Bragg angles of 30.09, 35.42, 37.05, 43.05, 53.39, 56.94 and 62.51 correspond to the (2 2 0), (3 1 1), (2 2 2), (4 0 0), (4 2 2), (5 1 1) and (4 4 0) facets of the cubic spinel crystal planes of Fe_3O_4 (JCPDS card No. 19-0629), respectively (Hou, Zhang, Zhu, Li, & Wang, 2011). The broad diffraction peaks are indications of the nanoparticles with very small sizes (Wang et al., 2013).

The FT-IR spectra of MGO, β-CD, and CD-E-MGO are shown in Fig. 2(b). The spectrum of MGO illustrates the presence of C=O in carboxylic acid and carbonyl moieties ($\nu_{C=O}$ at 1725 cm^{-1}), C—OH (ν_{C-OH} at 1387 cm^{-1}), C—O—C in the epoxy group (ν_{C-O-C} at 1050 cm^{-1}), Fe—O in Fe_3O_4 (ν_{Fe-O} at 560 cm^{-1}) (Bai et al., 2012; Hou et al., 2011; Ma et al., 2012; Si & Samulski, 2008). While in the FT-IR spectrum of CD-E-MGO, the band at 1657 cm^{-1} corresponds to the characteristic C=O stretching vibration of —NHCO— (amide I) (Konkena & Vasudevan, 2012). The stretching band of amide C—N peak and the amide N—H bending mode appear at 1239 and 1576 cm^{-1}, respectively (Konkena & Vasudevan, 2012). The peaks at 1028 and 942 cm^{-1} correspond to the antisymmetric glycosidic ν_a (C—O—C) vibrations (Badruddoza et al., 2013) and the R-1,4-bond skeleton vibration of β-CD, respectively (Fan et al., 2012). The characteristic sorption band of magnetic nanoparticles is 587 cm^{-1}, which is due to Fe—O bonds in the tetrahedral sites

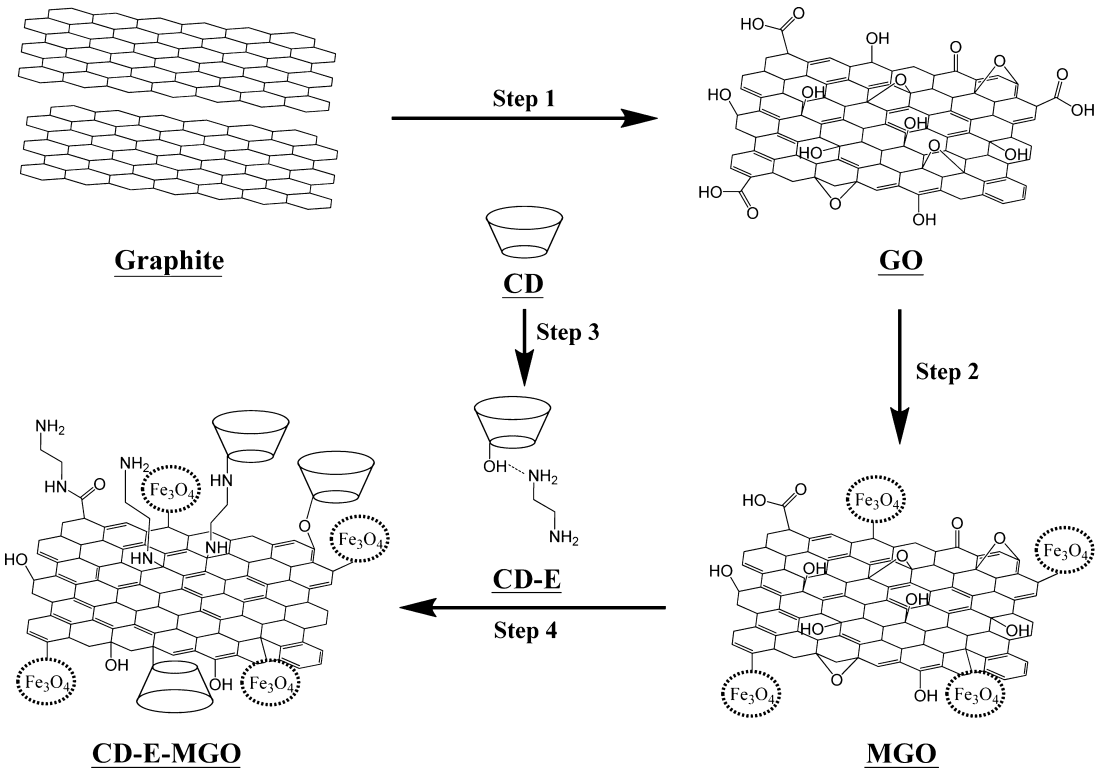

Fig. 1. The proposed scheme for the formation of CD-E-MGO: (Step 1) oxidation of natural graphite to graphite oxide, followed by ultrasonication; (Step 2) preparation of MGO by loading magnetic nanoparticles on the GO surfaces through chemical coprecipitation method; (Step 3) preparation of CD-E solution; (Step 4) formation of CD-E-MGO by grafting CD-E onto the MGO surfaces.

(Badruddoza et al., 2013). After the chemical grafting, the bands at 1725 cm^{-1} and 1050 cm^{-1} disappear for CD-E-MGO, demonstrating that β-CD and ethylenediamine mainly react with the carboxyl, carbonyl, and epoxide groups of MGO.

XPS analysis was performed on MGO before and after its reaction with ethylenediamine and β-CD, to gain further information on its chemical composition. From Fig. S2 (Supplementary data), three notable peaks assigned to C1s, O1s, and Fe2p are observed in the XPS survey scan spectra of MGO and CD-E-MGO. Moreover, XPS survey of CD-E-MGO shows significant amount of N1s comparing to that of MGO, which is originated from the grafted ethylenediamine. The elemental analysis illustrates a considerable increase in O/C atomic ratio in the CD-E-MGO (0.41) compared to that of the MGO (0.31), which may be attributed to the high O/C atomic ratio of the introduced β-CD. From Fig. 2(c), the C1s XPS spectrum of MGO clearly indicates a fairly high degree of oxidation with five components that correspond to carbon atoms: non-oxygenated ring C (284.6 eV), in the form of C—O (286.2 eV), C—O—C (epoxy group, 286.9 eV), C═O (carbonyl, 288.1 eV), and O—C═O (289.0 eV) (Che et al., 2010; Huang et al., 2011; Liu, Chen, & Jiang, 2011). As shown in Fig. 2(d), the C1s XPS spectrum of CD-E-MGO can be curve-fitted into five peak components at approximately 284.6, 285.5, 286.2, 287.7, and 288.2 eV, attributable to the C—H, C—N, C—O, C—O—C (in β-CD), and HNC═O (Min et al., 2012; Xu et al., 2010). The peaks at 286.5, 288.1, and 289.0 eV for CD-E-MGO are absent, which may be due to the reaction of the carboxyl, carbonyl, and epoxide groups of MGO with β-CD and ethylenediamine. Thus, it can be concluded that β-CD and ethylenediamine have been grafted successfully to the MGO surface.

As shown in Fig. 2(e), Raman spectra of GO and CD-E-MGO display two prominent peaks at ca. 1336 and 1593 cm^{-1}, which are assigned to the D band (related to the vibration of sp^3 carbon atoms of defects and disorder) and G band (associated with the vibration of sp^2 carbon atoms in a graphitic 2D hexagonal lattice), respectively (Zhao, Li, Ren, Chen, & Wang, 2011). It is well known that the intensity ratio of D (I_D) and G bands (I_G) can be used to measure the extent of disorder. The I_D/I_G of CD-E-MGO is slightly higher than that of the GO, which may be due to the introduction of β-CD to the sp^2 carbon network (Hu et al., 2013; Ji et al., 2011).

The room-temperature magnetization hysteresis curve was measured using vibrating sample magnetometry (VSM) to study the magnetic properties of CD-E-MGO. As shown in Fig. 2(f), the magnetic hysteresis loop is S-like curve. The saturation magnetization (M_s) of the CD-E-MGO composite is 17.49 emu/g, which is sufficient to be separated from aqueous solution by a permanent magnet. The retentivity (M_r) is 0.154 emu/g, nearly zero. This indicated that there is almost no remaining magnetization when the external magnetic field is removed, suggesting that CD-E-MGO composite exhibits a superparamagnetic behavior (Bai et al., 2012). The insets in Fig. 2(f) show that the CD-E-MGO can be collected from aqueous solution by a permanent magnet. This property is essentially important for the convenient recycling of the CD-E-MGO composite.

3.2. Cr(VI) sorption kinetics

The effects of contact time on decontamination of Cr(VI) by CD-E-MGO were investigated at three different initial Cr(VI) concentrations (10, 20, and 40 mg/L) and the results are shown in Fig. 3(a). The sorption capacities of CD-E-MGO for Cr(VI) increase quickly in the initial 60 min and then rise slowly until the sorption equilibrium is reached within 360 min. Further increase of contact time cannot lead to a stronger sorption capacity. Quantifying the changes in sorption with time requires an appropriate

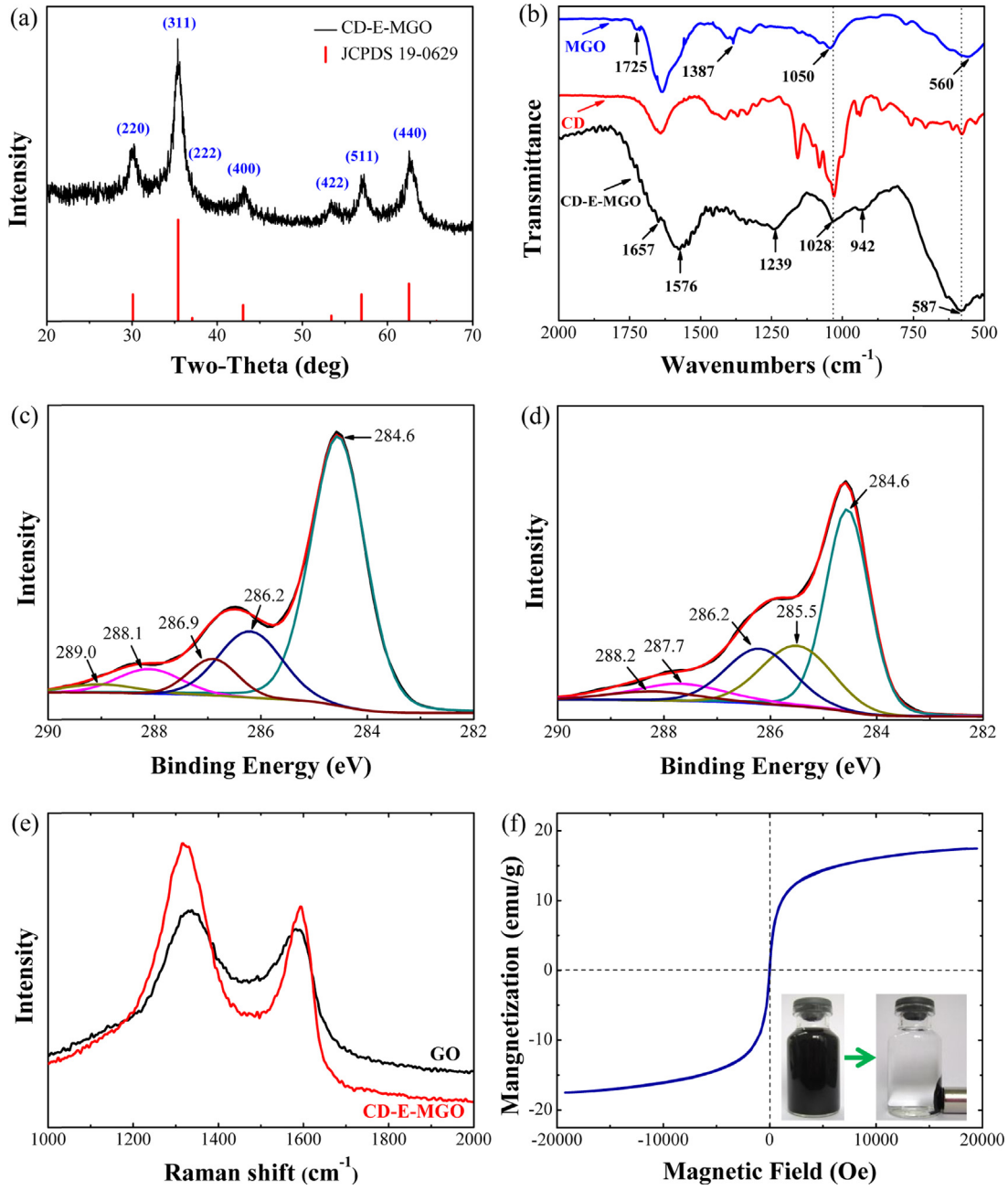

Fig. 2. (a) XRD pattern of CD-E-MGO; (b) FT-IR spectra of MGO, β-CD, and CD-E-MGO; C1s XPS spectra of (c) MGO and (d) CD-E-MGO; (e) Raman spectra of GO and CD-E-MGO; (f) Magnetization curve (The insets show the CD-E-MGO dispersed in ultrapure water and the magnetic separation).

Table 1
Kinetic parameters of Cr(VI) sorption on CD-E-MGO.

Kinetic parameter		10 mg/L	20 mg/L	40 mg/L
		$q_{e,exp}$ = 40.97	$q_{e,exp}$ = 50.69	$q_{e,exp}$ = 60.82
Pseudo-first-order model	k_1 (1/min)	2.69×10^{-3}	3.13×10^{-3}	2.44×10^{-3}
	$q_{e,1}$ (mg/g)	16.39	23.56	26.91
	R^2	0.899	0.940	0.866
	RMSE	11.865	10.443	12.592
	χ^2	1.408	1.091	1.586
Pseudo-second-order model	k_2 (g/mg min)	8.57×10^{-4}	6.05×10^{-4}	4.91×10^{-4}
	$q_{e,2}$ (mg/g)	40.88	50.97	60.42
	h (mg/g min)	1.432	1.572	1.792
	R^2	0.998	0.998	0.997
	RMSE	0.496	0.391	0.400
	χ^2	0.246	0.153	0.159

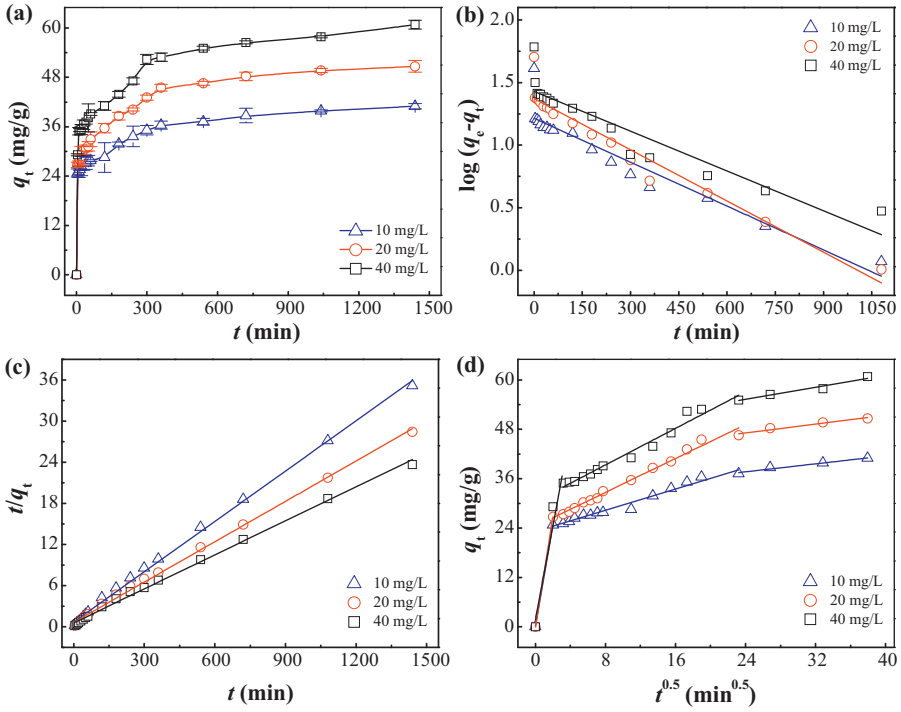

Fig. 3. (a) Time-dependent Cr(VI) sorption on CD-E-MGO at three different concentration (10, 20 and 40 mg/L); (b) Pseudo-first-order sorption kinetics; (c) Pseudo-second-order sorption kinetics; (d) Intraparticle diffusion kinetics; (m/V = 0.17 g/L, I = 0.002 M NaCl, pH = 3.0 ± 0.1, T = 30 °C, t = 24 h).

kinetic model, and therefore pseudo-first-order, pseudo-second-order and intraparticle diffusion models were investigated and compared. Detailed information of these models is described in the Supplementary data. Pseudo-first-order and pseudo-second-order sorption kinetics are shown in Fig. 3(b) and (c), respectively. The kinetic parameters calculated from the two models are listed in Table 1. It can be seen that the correlation coefficients of pseudo-second-order model are much higher than that of pseudo-first-order, and the error functions (*RMSE* and χ^2) of pseudo-second-order model are lower than that of pseudo-first-order. In addition, the calculated q_e values of pseudo-second-order model are found to agree very well with the experimental data. Therefore, the kinetic data for the sorption process obey the pseudo-second-order model, indicating that the rate-limiting step may be due to the chemical adsorption, high specific surface area and the absence of internal diffusion resistance (Fan et al., 2012; Plazinski, Rudzinski, & Plazinska, 2009; Zhao, Shen, Pan, & Hu, 2010). From Table 1, the constant rate k_2 decreases with the increase of initial Cr(VI) concentration, which indicates that the system with higher initial Cr(VI) concentration requires more time to reach the final equilibrium (Balan et al., 2013).

The intraparticle diffusion model was used to identify the mass transfer steps in the Cr(VI) decontamination by CD-E-MGO (Hu et al., 2013). Detailed information of this model is described in the Supplementary data. Fig. 3(d) shows q_t versus $t^{0.5}$ plots for the sorption of Cr(VI) at different initial Cr(VI) concentrations. Piecewise linear regression of the data shows that q_t versus $t^{0.5}$ plots have three distinct regions. The initial sharply curved portions may be attributed to the film diffusion. The second portions are the gradual sorption stage, where the intraparticle diffusion is the rate-limiting step. The final linear portions indicate the final equilibrium stages where the intraparticle diffusion starts to slow down due to the extremely low Cr(VI) concentrations in the solution and the fewer sorption sites of CD-E-MGO (Daifullah et al., 2007). Therefore, both film diffusion and intraparticle diffusion occur simultaneously, and the intraparticle diffusion is not the only rate controlling step for the whole process (Hu et al., 2013).

3.3. Sorption isotherms and thermodynamics

To better understand the sorption mechanisms, the Langmuir and Freundlich models, as described in the Supplementary data, were applied to simulate the experimental data. The Langmuir isotherm is often applicable to a homogeneous sorption surface with all the sorption sites having equal adsorbate affinity, while the Freundlich isotherm model assumes heterogeneity of sorption surfaces (Gong, Liu, Wang, Hu, & Zhang, 2011). The Langmuir and Freundlich sorption isotherms obtained using the non-linear method at 10, 30 and 50 °C are shown in Fig. 4. The related parameters of the two models are listed in Table 2. From the correlation coefficients (R^2) and the fitting curves, we can see that the Langmuir

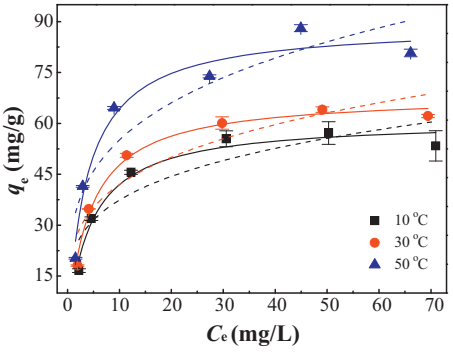

Fig. 4. Langmuir and Freundlich non-linear plots of sorption isotherms for Cr(VI) onto CD-E-MGO at 10, 30 and 50 °C. The solid lines are Langmuir model simulation, and the dashed lines are Freundlich model simulation (m/V = 0.17 g/L, I = 0.002 M NaCl, pH = 3.0 ± 0.1, t = 24 h).

Table 2
Parameters for Langmuir and Freundlich isotherm models at different temperatures.

T (°C)		10	30	50
Langmuir	q_{max} (mg/g)	60.95	68.41	89.15
	K_L (L/mg)	0.220	0.231	0.258
	R^2	0.966	0.986	0.961
	RMSE	2.978	2.148	5.137
	χ^2	8.871	4.615	26.385
Freundlich	K_F (L/mg)	21.21	23.41	30.11
	n	4.06	3.95	3.81
	R^2	0.790	0.844	0.835
	RMSE	7.346	7.240	10.504
	χ^2	54.001	52.417	110.339

model fits the experimental data better than the Freundlich model, indicating that monolayer coverage of CD-E-MGO is the main sorption mechanism (Hu et al., 2013). The value of q_{max} at 10, 30, and 50 °C are found to be 60.95, 68.41, and 89.15 mg/g, respectively, which are higher than that of β-CD polymers (21 mg/g, pH 6.5, 25 °C) (Sikder et al., 2012), chitosan-carboxymethyl-β-cyclodextrin (44.7 mg/g, pH 6.0, 25–50 °C) (Sikder et al., 2014) and magnetic cyclodextrin-chitosan/graphene oxide (55.0 mg/g, pH 3.0, 50 °C) (Li et al., 2013). The values of K_L for Cr(VI) sorption onto CD-E-MGO are 0.220, 0.231 and 0.258 L/mg at 10, 30 and 50 °C, respectively. Both q_{max} and K_L of the Langmuir model increase with the increasing of temperature, indicating that the sorption process is endothermic (Hu et al., 2011).

The thermodynamic parameters, including the standard free-energy change (ΔG°), standard enthalpy change (ΔH°) and standard entropy change (ΔS°), provide in-depth information about internal energy changes associated with sorption (Xu et al., 2012). These parameters can be calculated by using the equations, which are described in the Supplementary data. The values of ΔH° and ΔS° can be obtained from the slope and intercept of the plot of $\ln K^\circ$ against $1/T$ from Fig. S3. The calculated results are listed in Table S1 (Supplementary data). The negative ΔG° values (−5.85 kJ/mol at 10 °C, −5.27 kJ/mol at 30 °C, −3.47 kJ/mol at 50 °C) indicate that the sorption of Cr(VI) onto CD-E-MGO is a spontaneous process (Xu et al., 2012). The positive value of ΔH° (22.47 kJ/mol) suggests that the sorption is endothermic, which is in good agreement with the result that the sorption of Cr(VI) increases with the increasing of temperature (Fig. 4). The negative value of ΔS° (−58.11 J/K mol) reflects decreased randomness at the solid–liquid interface during the sorption of Cr(VI) on CD-E-MGO and also implies some structural changes in CD-E-MGO during sorption process (Li et al., 2012). The results imply that the sorption of Cr(VI) on CD-E-MGO is an endothermic and spontaneous process.

3.4. Effect of initial solution pH

Solution pH is a significant controlling factor in sorption process. Fig. 5(a) shows the influence of the pH on decontamination of Cr(VI) by CD-E-MGO and MGO. From Fig. 5(a), the sorption capacities of CD-E-MGO and MGO for Cr(VI) decrease gradually with the increase of pH values from 2.5 to 9.3, which indicates that the sorption of Cr(VI) by CD-E-MGO or MGO is clearly pH-dependent. It is well known that the solution pH affects the speciation of Cr(VI) and the surface charge of the sorbents. The speciation of Cr(VI) (10 mg/L) as a function of solution pH was obtained using the program visual MINTEQ. As shown in Fig. 5(b), different forms of Cr(VI) such as H_2CrO_4(aq), $Cr_2O_7^-$, $HCrO_4^-$, $KCrO_4^-$ and CrO_4^{2-} coexist in the aqueous solution. $HCrO_4^-$ is the predominant Cr(VI) species at pH < 6.51, while CrO_4^{2-} is predominant at pH > 6.51. Simultaneously, the surface charge of adsorbent can be affected by the solution pH. As shown in Fig. S4, the zeta potential of CD-E-MGO decreases with the increase of pH. At pH < 6.16, the zeta potentials of CD-E-MGO are positive. At pH > 6.16, the surfaces of CD-E-MGO are negatively charged. The pH_{pzc} value of MGO is 4.65 as reported by Li et al. (2012). In low pH environments, the

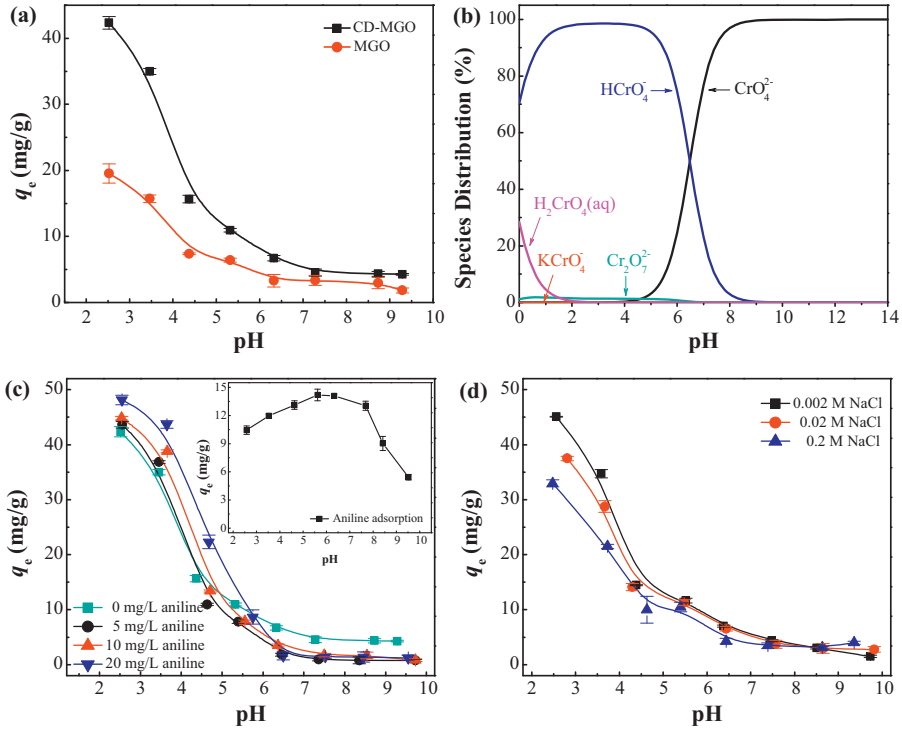

Fig. 5. (a) pH profile of Cr(VI) sorption on CD-E-MGO; (b) Distribution of Cr(VI) species ($C_{Cr(VI)}$ = 10 mg/L) in solution as a function of pH computed by the program visual MINTEQ; (c) Effect of aniline on Cr(VI) sorption (The inset shows the aniline adsorption by CD-E-MGO from system with 10 mg/L Cr(VI) and 10 mg/L aniline); (d) Effect of ionic strength on Cr(VI) sorption ($C_{Cr(VI)\ initial}$ = 10 mg/L, m/V = 0.17 g/L, T = 30 °C, t = 24 h).

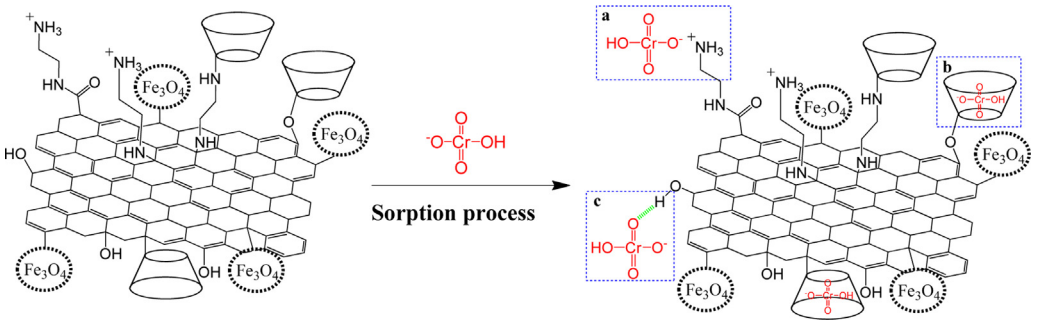

Fig. 6. Schematic of (a) electrostatic attraction, (b) host–guest interactions and (c) hydrogen bonding between Cr(VI) ions ($HCrO_4^-$) and CD-E-MGO.

positively charged surfaces of MGO and CD-E-MGO readily attract the negative charged Cr(VI) ions ($HCrO_4^-$) by electrostatic forces. With increasing pH, the buildup of negative charge on the CD-E-MGO and MGO surfaces results in a prevailing electrostatic repulsion between Cr(VI) ions (CrO_4^{2-}) and the sorbents, which consequently reduces the Cr(VI) sorption. Besides, in high pH environments, there is a high concentration of OH^-, which can compete with Cr(VI) ions for the binding sites on the surfaces of the sorbents, resulting in a decreased sorption of Cr(VI) (Hu et al., 2013). Fig. 5(a) also shows that the sorption of Cr(VI) on CD-E-MGO is higher than that of Cr(VI) on MGO at the same solid content. The introduction of β-CD and ethylenediamine to the MGO surface can increase the sorption capacity of CD-E-MGO for Cr(VI) ions.

3.5. Effect of aniline

Aniline and Cr(VI) ions are common co-existing contaminants in wastewater. As seen in Fig. 5(c), the presence of aniline affects the sorption properties of Cr(VI) on CD-E-MGO. In low pH environments, Cr(VI) sorption increases with increasing aniline concentration from 0 to 20 mg/L. This phenomenon can be explained by the complexation of Cr(VI) ions with the adsorbed aniline on CD-E-MGO surfaces. The inset in Fig. 5(c) shows that some aniline can be adsorbed by the CD-E-MGO from aqueous solution. The main interaction mechanism between aniline and CD-E-MGO is π–π electron coupling (Wu et al., 2011). The amino group on the benzene ring of the adsorbed aniline can form stable complexes with Cr(VI) ions, which increases the sorption sites of the CD-E-MGO for Cr(VI), thereby resulting in a more favorable attraction for Cr(VI) ions (Yang, Hu, Chen, Shao, & Wang, 2011). However, the sorption capacities of CD-E-MGO for Cr(VI) ions are reduced in the presence of aniline at high pH values. This can be interpreted by the formation of soluble Cr(VI)-aniline complexes in aqueous solution. From the inset in Fig. 5(c), the sorption of aniline on CD-E-MGO is reduced in the alkaline pH range, which may be due to the repulsive electrostatic interactions established between the negatively charged surfaces of CD-E-MGO and the aniline anions (Xu et al., 2012). This means that there are more aniline molecules in the aqueous solution at higher pH values, and these aniline molecules can form Cr(VI)-aniline complexes with Cr(VI) ions. More aniline in the aqueous solution indicates that there are fewer Cr(VI)-aniline complexes on the surfaces of CD-E-MGO.

3.6. Effect of ionic strength

The effect of ionic strength on the sorption of Cr(VI) on CD-E-MGO was studied by carrying out a series of experiments at three different NaCl concentrations. As illustrated in Fig. 5(d), the sorption of Cr(VI) on CD-E-MGO decreases as the NaCl concentration increases from 0.002 to 0.2 M. This phenomenon can be explained in terms of three aspects. First, competition of Cl^- with the Cr(VI) anion for sorption sites of CD-E-MGO results in the observed decrease in the uptake capacities with increasing NaCl concentration (Wang, Huang, Hu, Wang, & Qin, 2007). Second, the increase of NaCl concentration increases the screening effect between the negative charged Cr(VI) ions in solution and the positive charge on CD-E-MGO surfaces, which reduces the electrostatic interactions (Moreno-Castilla, Alvarez-Merino, Lopez-Ramon, & Rivera-Utrilla, 2004). Third, the ionic strength of solution influences the activity coefficient of Cr(VI) ions, which limits their transfers to CD-E-MGO surfaces (Ravat, Dumonceau, & Monteil-Rivera, 2000). Fig. S5 shows the effect of foreign anions on the Cr(VI) removal as a function of pH values in 0.02 M NaCl, $NaNO_3$, and $NaClO_4$ solutions. The sorption capacity of Cr(VI) on the CD-E-MGO is the highest in $NaClO_4$ solution at pH < 6, and no drastic difference of Cr(VI) sorption in the foreign anion solutions is observed at pH > 6. Based on the above theories and discussions, we can deduce that electrostatic attraction, host–guest interactions and hydrogen bonding are the main mechanisms for the removal of Cr(VI) onto CD-E-MGO. The first possible mechanism is sorption by electrostatic forces of the positively charged CD-E-MGO and the negative charge of the $HCrO_4^-$ (Hu et al., 2011). Besides, the β-CD grafted on the MGO surfaces can form inclusion complexes with Cr(VI) ions in its hydrophobic cavity through host–guest interactions (Szejtli, 1998). In addition to the above two possible mechanisms, another possible interaction is the hydrogen bonding between $HCrO_4^-$ and surface groups of CD-E-MGO (Xu et al., 2012). The schematic of the three interactions is shown in Fig. 6.

4. Conclusions

The analysis results of XRD, FTIR, Raman, magnetization property, and XPS indicated that CD-E-MGO composite was successfully synthesized. The CD-E-MGO exhibits superparamagnetic behavior and can be separated from the medium by magnetic separation. The sorption kinetics studies illustrated that the kinetics data can be well described with pseudo-second-order model, and both film diffusion and intraparticle diffusion simultaneously occur during the sorption processes. The equilibrium data can be well fitted with Langmuir model. The sorption reaction is an endothermic and spontaneous process. Decontamination of Cr(VI) was found to be more effective in the lower pH range and at higher temperatures. The graft of β-CD and ethylenediamine to MGO surfaces can increase the sorption capacity of CD-E-MGO. Besides, the presence of aniline in the solution can improve the sorption process, while the high pH range is unfavorable. The increasing ionic strength has a negative influence on the sorption capacity of CD-E-MGO. The large sorption affinity of CD-E-MGO for Cr(VI) ions may be due to that the negative charge of Cr(VI) ions can generate electrostatic interactions, host–guest interactions and hydrogen bonds with the hydrophobic cavity of β-CD and the functional groups of the sorbent. This

research indicates that CD-E-MGO is an effective sorbent for Cr(VI) decontamination from aqueous solution.

Acknowledgements

The authors would like to thank financial support from the National Natural Science Foundation of China (41271332), the Natural Science Foundation of Hunan province, China (11JJ2031), the Science and Technology Planning Project of Hunan Province, China (2012SK2021), and the Hunan Provincial Innovation Foundation For Postgraduate (CX2012B138).

Appendix A. Supplementary data

Supplementary data associated with this article can be found, in the online version, at http://dx.doi.org/10.1016/j.carbpol.2014.07.014.

References

Allen, M. J., Tung, V. C., & Kaner, R. B. (2009). Honeycomb carbon: A review of graphene. *Chemical Reviews*, *110*, 132–145.

Badruddoza, A. M., Shawon, Z. B., Daniel, T. W. J., Hidajat, K., & Uddin, M. S. (2013). Fe_3O_4/cyclodextrin polymer nanocomposites for selective heavy metals removal from industrial wastewater. *Carbohydrate Polymers*, *91*, 322–332.

Bai, L. Z., Zhao, D. L., Xu, Y., Zhang, J. M., Gao, Y. L., Zhao, L. Y., et al. (2012). Inductive heating property of graphene oxide-Fe_3O_4 nanoparticles hybrid in an AC magnetic field for localized hyperthermia. *Materials Letters*, *68*, 399–401.

Balan, C., Volf, I., & Bilba, D. (2013). Chromium(VI) removal from aqueous solutions by purolite base anion-exchange resins with gel structure. *Chemical Industry & Chemical Engineering Quarterly*, *19*, 615–628.

Che, J., Shen, L., & Xiao, Y. (2010). A new approach to fabricate graphene nanosheets in organic medium: Combination of reduction and dispersion. *Journal of Materials Chemistry*, *20*, 1722–1727.

Chen, C.-Y., Chen, C.-C., & Chung, Y.-C. (2007). Removal of phthalate esters by α-cyclodextrin-linked chitosan bead. *Bioresource Technology*, *98*, 2578–2583.

Chen, G. F., Zhai, S. Y., Zhai, Y. L., Zhang, K., Yue, Q. L., Wang, L., et al. (2011). Preparation of sulfonic-functionalized graphene oxide as ion-exchange material and its application into electrochemiluminescence analysis. *Biosensors & Bioelectronics*, *26*, 3136–3141.

Daifullah, A. A. M., Yakout, S. M., & Elreefy, S. A. (2007). Adsorption of fluoride in aqueous solutions using $KMnO_4$-modified activated carbon derived from steam pyrolysis of rice straw. *Journal of Hazardous Materials*, *147*, 633–643.

Fan, L., Zhang, Y., Luo, C., Lu, F., Qiu, H., & Sun, M. (2012). Synthesis and characterization of magnetic β-cyclodextrin-chitosan nanoparticles as nano-adsorbents for removal of methyl blue. *International Journal of Biological Macromolecules*, *50*, 444–450.

Gong, J. M., Liu, T., Wang, X. Q., Hu, X. L., & Zhang, L. Z. (2011). Efficient removal of heavy metal ions from aqueous systems with the assembly of anisotropic layered double hydroxide nanocrystals@carbon nanosphere. *Environmental Science & Technology*, *45*, 6181–6187.

Guo, L., Li, G., Liu, J., Yin, P., & Li, Q. (2009). Adsorption of aniline on cross-linked starch sulfate from aqueous solution. *Industrial & Engineering Chemistry Research*, *48*, 10657–10663.

Guo, Y., Guo, S., Li, J., Wang, E., & Dong, S. (2011). Cyclodextrin–graphene hybrid nanosheets as enhanced sensing platform for ultrasensitive determination of carbendazim. *Talanta*, *84*, 60–64.

Guo, Y., Guo, S., Ren, J., Zhai, Y., Dong, S., & Wang, E. (2010). Cyclodextrin functionalized graphene nanosheets with high supramolecular recognition capability: Synthesis and host–guest inclusion for enhanced electrochemical performance. *ACS Nano*, *4*, 4001–4010.

Hou, C., Zhang, Q., Zhu, M., Li, Y., & Wang, H. (2011). One-step synthesis of magnetically-functionalized reduced graphite sheets and their use in hydrogels. *Carbon*, *49*, 47–53.

Hu, X.-j., Liu, Y.-g., Wang, H., Chen, A.-w., Zeng, G.-m., Liu, S.-m., et al. (2013). Removal of Cu(II) ions from aqueous solution using sulfonated magnetic graphene oxide composite. *Separation and Purification Technology*, *108*, 189–195.

Hu, X.-j., Wang, J.-s., Liu, Y.-g., Li, X., Zeng, G.-m., Bao, Z.-l., et al. (2011). Adsorption of chromium(VI) by ethylenediamine-modified cross-linked magnetic chitosan resin: Isotherms, kinetics and thermodynamics. *Journal of Hazardous Materials*, *185*, 306–314.

Huang, Z.-H., Zheng, X., Lv, W., Wang, M., Yang, Q.-H., & Kang, F. (2011). Adsorption of lead(II) ions from aqueous solution on low-temperature exfoliated graphene nanosheets. *Langmuir*, *27*, 7558–7562.

Ji, J., Zhang, G., Chen, H., Wang, S., Zhang, G., Zhang, F., et al. (2011). Sulfonated graphene as water-tolerant solid acid catalyst. *Chemical Science*, *2*, 484–487.

Konkena, B., & Vasudevan, S. (2012). Covalently linked, water-dispersible cyclodextrin: Reduced-graphene oxide sheets. *Langmuir*, *28*, 12432–12437.

Li, J., Zhang, S., Chen, C., Zhao, G., Yang, X., Li, J., et al. (2012). Removal of Cu(II) and fulvic acid by graphene oxide nanosheets decorated with Fe_3O_4 nanoparticles. *ACS Applied Materials & Interfaces*, *4*, 4991–5000.

Li, L., Fan, L., Sun, M., Qiu, H., Li, X., Duan, H., et al. (2013). Adsorbent for chromium removal based on graphene oxide functionalized with magnetic cyclodextrin-chitosan. *Colloids and Surfaces B: Biointerfaces*, *107*, 76–83.

Lin, X. Y., Zhang, J. P., Luo, X. G., Zhang, C., & Zhou, Y. (2011). Removal of aniline using lignin grafted acrylic acid from aqueous solution. *Chemical Engineering Journal*, *172*, 856–863.

Liu, J., Chen, G., & Jiang, M. (2011). Supramolecular hybrid hydrogels from noncovalently functionalized graphene with block copolymers. *Macromolecules*, *44*, 7682–7691.

Ma, H. L., Zhang, Y. W., Hu, Q. H., Yan, D., Yu, Z. Z., & Zhai, M. L. (2012). Chemical reduction and removal of Cr(VI) from acidic aqueous solution by ethylenediamine-reduced graphene oxide. *Journal of Materials Chemistry*, *22*, 5914–5916.

Madadrang, C. J., Kim, H. Y., Gao, G., Wang, N., Zhu, J., Feng, H., et al. (2012). Adsorption behavior of EDTA-graphene oxide for Pb(II) removal. *ACS Applied Materials & Interfaces*, *4*, 1186–1193.

Min, H., Girard-Lauriault, P.-L., Gross, T., Lippitz, A., Dietrich, P., & Unger, W. S. (2012). Ambient-ageing processes in amine self-assembled monolayers on microarray slides as studied by ToF-SIMS with principal component analysis XPS, and NEXAFS spectroscopy. *Analytical and Bioanalytical Chemistry*, *403*, 613–623.

Moreno-Castilla, C., Alvarez-Merino, M. A., Lopez-Ramon, M. V., & Rivera-Utrilla, J. (2004). Cadmium ion adsorption on different carbon adsorbents from aqueous solutions. Effect of surface chemistry, pore texture, ionic strength, and dissolved natural organic matter. *Langmuir*, *20*, 8142–8148.

NSPRC. (1987). *Water Quality—Determination of Chromiun(VI)—1,5-Diphenylcarbohydrazide Spectrophotometric Method*. NSPRC. GB 7467-87

Ohashi, H., Hiraoka, Y., & Yamaguchi, T. (2006). An autonomous phase transition-complexation/decomplexation polymer system with a molecular recognition property. *Macromolecules*, *39*, 2614–2620.

Ozmen, E. Y., Sezgin, M., Yilmaz, A., & Yilmaz, M. (2008). Synthesis of β-cyclodextrin and starch based polymers for sorption of azo dyes from aqueous solutions. *Bioresource Technology*, *99*, 526–531.

Pan, J., Zou, X., Wang, X., Guan, W., Li, C., Yan, Y., et al. (2011). Adsorptive removal of 2,4-didichlorophenol and 2,6-didichlorophenol from aqueous solution by β-cyclodextrin/attapulgite composites: Equilibrium, kinetics and thermodynamics. *Chemical Engineering Journal*, *166*, 40–48.

Plazinski, W., Rudzinski, W., & Plazinska, A. (2009). Theoretical models of sorption kinetics including a surface reaction mechanism: A review. *Advances in Colloid and Interface Science*, *152*, 2–13.

Ravat, C., Dumonceau, J., & Monteil-Rivera, F. (2000). Acid/base and Cu(II) binding properties of natural organic matter extracted from wheat bran: Modeling by the surface complexation model. *Water Research*, *34*, 1327–1339.

Si, Y., & Samulski, E. T. (2008). Synthesis of water soluble graphene. *Nano Letters*, *8*, 1679–1682.

Sikder, M. T., Kikuchi, T., Suzuki, J., Hosokawa, T., Saito, T., & Kurasaki, M. (2012). Removal of cadmium and chromium ions using modified α β, and γ-cyclodextrin polymers. *Separation Science and Technology*, *48*, 587–597.

Sikder, M. T., Mihara, Y., Islam, M. S., Saito, T., Tanaka, S., & Kurasaki, M. (2014). Preparation and characterization of chitosan-caboxymethyl-β-cyclodextrin entrapped nanozero-valent iron composite for Cu(II) and Cr(IV) removal from wastewater. *Chemical Engineering Journal*, *236*, 378–387.

Szejtli, J. (1998). Introduction and general overview of cyclodextrin chemistry. *Chemical Reviews*, *98*, 1743–1754.

Wang, X.-S., Huang, J., Hu, H.-Q., Wang, J., & Qin, Y. (2007). Determination of kinetic and equilibrium parameters of the batch adsorption of Ni(II) from aqueous solutions by Na-mordenite. *Journal of Hazardous Materials*, *142*, 468–476.

Wang, Y., Michel, M., Levard, C., Choi, Y., Eng, P. J., & Brown, G. E. (2013). Competitive sorption of Pb(II) and Zn(II) on polyacrylic acid-coated hydrated aluminum-oxide surfaces. *Environmental Science & Technology*, *47*, 12131–12139.

Wu, T., Cai, X., Tan, S., Li, H., Liu, J., & Yang, W. (2011). Adsorption characteristics of acrylonitrile, *p*-toluenesulfonic acid, 1-naphthalenesulfonic acid and methyl blue on graphene in aqueous solutions. *Chemical Engineering Journal*, *173*, 144–149.

Xu, J., Wang, L., & Zhu, Y. F. (2012). Decontamination of bisphenol A from aqueous solution by graphene adsorption. *Langmuir*, *28*, 8418–8425.

Xu, L. Q., Wan, D., Gong, H. F., Neoh, K.-G., Kang, E.-T., & Fu, G. D. (2010). One-pot preparation of ferrocene-functionalized polymer brushes on gold substrates by combined surface-initiated atom transfer radical polymerization and click chemistry. *Langmuir*, *26*, 15376–15382.

Yang, S. B., Hu, J., Chen, C. L., Shao, D. D., & Wang, X. K. (2011). Mutual effects of Pb(II) and humic acid adsorption on multiwalled carbon nanotubes/polyacrylamide composites from aqueous solutions. *Environmental Science & Technology*, *45*, 3621–3627.

Yang, S. T., Chang, Y. L., Wang, H. F., Liu, G. B., Chen, S., Wang, Y. W., et al. (2010). Folding/aggregation of graphene oxide and its application in Cu^{2+} removal. *Journal of Colloid and Interface Science*, *351*, 122–127.

Zhao, G., Li, J., Ren, X., Chen, C., & Wang, X. (2011). Few-layered graphene oxide nanosheets as superior sorbents for heavy metal ion pollution management. *Environmental Science & Technology*, *45*, 10454–10462.

Zhao, Y.-G., Shen, H.-Y., Pan, S.-D., & Hu, M.-Q. (2010). Synthesis, characterization and properties of ethylenediamine-functionalized Fe_3O_4 magnetic polymers for removal of Cr(VI) in wastewater. *Journal of Hazardous Materials*, *182*, 295–302.